Journal of Power Sources 240 (2013) 536–543

Contents lists available at SciVerse ScienceDirect

Journal of Power Sources

journal homepage: www.elsevier.com/locate/jpowsour

Self-assembly of highly dispersed Pt and PtRu nanoparticles on perylene diimide derivatives functionalized carbon nanotubes as enhanced catalysts for methanol electro-oxidation

Xiulin Yang [a,b], Xianzong Liu [a,b], Xiangyue Meng [a,b], Xueyun Wang [a,b], Gen Li [a,b], Chunying Shu [a], Li Jiang [a,*], Chunru Wang [a,*]

[a] Beijing National Laboratory for Molecular Sciences, Key Lab of Molecular Nanostructure and Nanotechnology, Institute of Chemistry, Chinese Academy of Sciences, Beijing 100190, China
[b] University of Chinese Academy of Sciences, Beijing 100039, China

HIGHLIGHTS

- One-pot solvothermal method synthesized perylene diimides derivatives (PD) molecule.
- The PD molecule functionalized on CNTs via π–π stacking.
- The Pt-based NPs self-assembled on CNTs surface by electrostatic interaction.
- The as-prepared catalyst revealed excellent catalytic performance for methanol electro-oxidation.

GRAPHICAL ABSTRACT

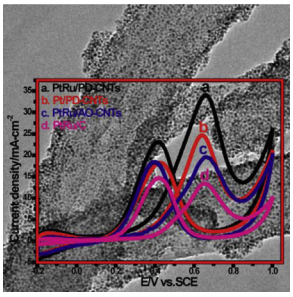

ARTICLE INFO

Article history:
Received 6 January 2013
Received in revised form
15 April 2013
Accepted 16 April 2013
Available online 25 April 2013

Keywords:
Self-assembly
Perylene diimide
Carbon nanotubes
Electrocatalysis
Fuel cells

ABSTRACT

Both narrow size and highly homogeneous distribution of Pt and PtRu nanoparticles (NPs) are achieved on multi-walled carbon nanotubes functionalized by perylene diimide derivatives (PD-CNTs) using ethylene glycol as reducing agents. FT-IR and UV–visible spectrum illustrate that the PA molecule has been successfully transformed into PD molecule and modified on the surface of CNTs. TEM images show that a multilayer of the PD moiety is formed on CNT surface followed by the uniform deposition of Pt and PtRu NPs through self-assembly. The resulting Pt and PtRu NPs on PD-CNTs exhibit competitively catalytic activity for methanol electro-oxidation and outstanding CO-tolerance properties compared to PtRu NPs on acid-oxidized CNTs (AO-CNTs) and carbon black. Furthermore, the PD-CNT based catalysts are also much more stable than PtRu/AO-CNTs through long-term cycle stability testing. The proposed synthesis route provides a facile, feasible and effective method for developing highly efficient electrocatalysts.

1. Introduction

Both energy dilemma and environmental crisis make it imperative to investigate alternative energy sources [1,2]. Direct methanol fuel cells (DMFCs) are regarded as a high-efficiency, low-emission and inexpensive future source for powering portable electronics by converting the chemical energy of methanol directly into electricity [3,4]. The low catalytic activity of electrodes for the methanol oxidation reaction, however, keeps being one of bottlenecks to hinder the development of DMFCs [5,6]. Many efforts are required to be made on both catalyst dispersion and carbon-support design, aiming at enhancing the catalytic activity [7,8].

* Corresponding authors.
E-mail addresses: jiangli@iccas.ac.cn (L. Jiang), crwang@iccas.ac.cn (C. Wang).

0378-7753/$ – see front matter © 2013 Elsevier B.V. All rights reserved.
http://dx.doi.org/10.1016/j.jpowsour.2013.04.084

Since the discovery of CNTs, researches have focused on the exploration of their unique structure and electrical properties relevant to technological applications in the fields of nanoelectronic devices [9], hydrogen storage [10], advanced sensors [11], highly efficient fuel cells [12], *etc*. However, when it is as supporting materials for fuel cells, the purification and modification of the pristine CNTs are extremely important since the inert surface of CNTs would result in a poor dispersion of metal particles due to being short of active sites on it [13]. Active sites on the surface of CNTs are generally provided via surface functionalization, such as chemical oxidation to generate defects on the sidewalls and tube tips [14,15], polymer directly grafting on the surface of the CNTs [16,17], in situ polymerization and physically adsorbed polymer chain on CNT surface [18,19], and noncovalent functionalization of aromatic molecule by π stacking [20,21], *etc*.

N-doped carbon nanomaterials have shown improved catalytic and electrochemical performances, such as nitrogen-doped microporous activated carbon [22,23], porous carbon nanospheres [24], carbon nanotube cups [25], and CNTs [26,27], *etc*. In the present study, we report another novel metal NPs/nitrogen-containing surface functional CNT catalyst, which electron-conductive PD is introduced to bridge metal NPs and CNTs. Compared to the 3,4,9,10-perylene tetracarboxylic acid-functionalized graphene sheets supported metal NPs catalysts reported [28], the PD modified CNTs in this study revealed following advantages: 1) better dispersion and narrower size distribution of metal NPs, 2) higher electrocatalytic properties and stabilities, and 3) higher efficiency of anti-poisoning tolerance to the incomplete oxidized species during methanol oxidation.

2. Experimental section

2.1. Materials

All chemical reagents used in this experiment were of analytical grade. H_2SO_4, HNO_3, $H_2PtCl_6{\cdot}6H_2O$, $RuCl_3$, CH_2Cl_2, $(CH_3CH_2)_3N$, methanol, ethanol and ethylene glycol, ethylenediamine, perylene-3, 4, 9, 10-tetracarboxylic dianhydride (PA) were procured commercially and were used as received without further purification. The Raw-CNTs were purchased from Shenzhen Nanotechnologies Port Co. Ltd. (Shenzhen, China) with the diameters of 20–40 nm, lengths of 5–15 μm, and purity of 95%. Vulcan XC-72 carbon black was purchased from Cabot Corporation.

2.2. Synthesis of Pt and PtRu NPs on PD-CNTs

The synthetic route to obtain stable CNT-supported Pt and PtRu NPs starts by functionalization of the CNTs with the PD. Multi-walled CNTs (200 mg) and perylene-3, 4, 9, 10-tetracarboxylic dianhydride (50 mg) are dispersed in aqueous solution of CH_2Cl_2 (50 mL) containing $(CH_2NH_2)_2$ (2 mL) and $(CH_3CH_2)_3N$ (10 mL) with ultrasonication to ensure the presence of dispersed individual nanotubes. After ultrasonic treatment for 60 min, the obtained solution was then vigorous stirring at room temperature for another three days. The above solution was filtered using a nylon membrane with 0.22 μm pore-size and washed with double-distilled water and ethanol several times to thoroughly remove physically absorbed PD and unreacted monomer from the surface of the CNTs. The as-functionalized CNTs were dried in a vacuum oven at 70 °C for 10 h and collected (denoted as PD-CNTs).

Deposition of PtRu NPs on the walls of the PD-functionalized CNTs (20 wt% metal content, atomic ratio of Pt:Ru = 1:1) were achieved via polyol reduction process. The details were as follows: 40 mg of PD-CNTs with 1.78 mL of H_2PtCl_6 (18.97 mM) and 0.93 mL of $RuCl_3$ (36.31 mM) were placed in a 100 mL round bottom flask, to which 45.0 mL of ethylene glycol–water solution (2:1, v/v ratio) was added. The reduction reactions were performed under reflux conditions for 4 h with continuous magnetic stirring. After that, the mixture was filtered through a nylon membrane, and washed with double-distilled water and ethanol several times. The obtained PtRu/PD-CNTs were dried in a vacuum oven at 70 °C for 12 h. The deposition of Pt NPs on the PD-CNTs were carried out according to the same procedure except the precursor of metal NPs was changed from 1.78 mL of H_2PtCl_6 (18.97 mM) to 2.70 mL of H_2PtCl_6 (18.97 mM). The final products were labeled as Pt/PD-CNTs. PtRu NPs on acid-oxidized CNTs (PtRu/AO-CNTs) and carbon black (PtRu/C) were prepared using similar procedures as described above.

2.3. Characterization

MALDI-TOF MS (AXIMA Assurance, Japan) was used to study the structure of PD molecule, Fourier transform infrared spectrometry (FT-IR) (Thermo Fisher Scientific, America) was employed to analyze the surface chemical composition of the purified PD-CNT composite, UV–visible spectroscopy (Hitachi U-3010) was used to confirm the existence of PD after PD functionalization of CNTs, the weight percentage of PD to CNTs was determined using a thermal gravity analyzer (TGA) (STA 409 PC, Germany) with a rising temperature rate of 10 °C min^{-1} from 50 to 1000 °C under continuous N_2 flow. X-ray photoelectron spectroscopy (XPS) data was recorded with an ESCALab220i-XL electron spectrometer from VG Scientific using 300W Al Kα radiation, in which the binding energies were referenced to the C1s line at 284.8 eV from adventitious carbon. The morphology and microstructure of the synthesized materials were investigated by TEM (JEM-2010, Japan).

2.4. Electrochemical measurement

The electrochemical activity of PtRu/PD-CNT, Pt/PD-CNT, PtRu/AO-CNT, and PtRu/C electrocatalysts was measured for the electro-oxidation of methanol. As a typical process, 2.0 mg of electrocatalysts sample was ultrasonically mixed in 400 μL of ethanol–water solution (1:1, v/v ratio) to form a homogeneous ink followed by dropping 5 μL of the electrocatalysts ink onto the surface of a glassy carbon electrode (GCE, with a diameter of 3 mm). Then, 7 μL of Nafion solution of 1.0% in ethanol was added to fix the electrocatalysts on the GCE surface. Pt sheet and a saturated calomel electrode (SCE) were used as the counter and reference electrodes, respectively. All potentials in the present study were given versus SCE reference electrode. The electrochemical active surface (EAS) area was assessed using CO stripping techniques in 0.5 M H_2SO_4 solution. Initially, nitrogen was purged to the 0.5 M H_2SO_4 solution for 15 min. Afterwards, the adsorption of CO was performed by purging high-purity CO (99.9% purity) gas to the solution for 10 min while maintaining the potential at −0.16 V. Then, the dissolved CO in the solution was removed by bubbling nitrogen gas into the solution for 15 min by holding the potential at −0.16 V. Finally, the stripping voltammograms were collected between −0.2 and 1.0 V with a scan rate of 50 mV s^{-1}. The elelctrocatalytic activity for the methanol oxidation reaction was measured in a nitrogen-saturated 0.5 M H_2SO_4 + 1.0 M CH_3OH solution at a scan rate of 50 mV s^{-1}. Several activation scans were performed until reproducible voltammograms were obtained, and only the last cycles were used for comparison of the catalytic activity. The Pt metal loading was kept at 3.29 μg for PtRu (5.0 μg for Pt) and all tests were conducted at ambient temperature (25 ± 0.5 °C).

3. Results and discussion

3.1. Mechanism about formation of Pt and PtRu/PD-CNT catalysts

In order to understand the formation mechanism of the Pt and PtRu NPs on PD functionalized CNTs, the synthetic procedures are shown in Scheme 1. In the first step, 3,4,9,10-Perylene tetracarboxylic dianhydride and CNTs are one-pot dispersed into a mixture solution containing dichloromethane, triethylamine and ethylenediamine, in which the perylene tetracarboxylic dianhydride would transform into perylene diimide accompanied with the aromatic groups interacting with the sidewalls of CNTs *via* π–π stacking [29,30]. PD functionalized CNTs could not only introduce a large number of highly dispersed amino groups on the CNT surface but also lessen structural damage of CNTs compared with the conventional acid-oxidized method. Moreover, strong π–π stacking interaction make the amino groups of PD immobilize on the CNT surface to take on weakly positive charge, which can attract negative charges such as chloroplatinic acid ($PtCl_6^{2-}$) when added into the mixture. Then another positive charges (with and without Ru^{3+}) will be subsequently self-assembled through electrostatic interaction and coordination [27]. The resulted assembly complexes were refluxed at 140 °C for 4 h in ethylene glycol to form Pt or PtRu NPs loaded on the surface of PD-CNTs. As a comparison, PtRu NPs on acid-oxidized CNTs (PtRu/AO-CNTs) and carbon black (PtRu/C) were also investigated using the same self-assembly method. The synthesized PD molecule without addition CNTs was characterized by MALDI-TOF mass spectra with the parent molecular ion peaks appearing at *m*/*z* 476.13, which is consistent with the theoretical value of exact mass. The color change of PA and PD and the MALDI-TOF mass spectra of PD molecules are shown in Supporting information Fig. S1.

3.2. Morphological and crystal structure characterization catalysts

Fig. 1 shows TEM images and EDX spectrum of the Pt/PD-CNT and PtRu/PD-CNT nanohybrids. As a comparison, the TEM images of the PD-CNT alone and PtRu/AO-CNT nanocomposites are also presented. The coating of PD on the CNT surface was directly observed by TEM in Fig. 1a. A thin amorphous-like layer with the thickness of 2–7 nm covers the CNT surface, which indicates formation of a multilayer of the PD moiety. TEM images of Pt and PtRu NPs on PD functionalized CNTs are shown in Fig. 1b and c, respectively. It can be observed clearly that the Pt and PtRu NPs are homogeneously decorated on the outer surface of PD functionalized CNTs. A statistical size distribution obtained from 200 randomly selected NPs on PD-CNT support shows that the size distribution of the Pt NPs is quite narrow with an average diameter of ca. 2.3 nm (2.1 nm for PtRu NPs) without obvious aggregation in the whole images (see Supporting information Fig. S2a and b). The EDX spectra of Pt and PtRu NPs on PD-CNT support clearly show the presence of Pt (Ru), C, N and O element, which is consistent with the chemical composition of the as-prepared catalysts (Fig. 1e and f). The Cu signal is originated from the copper grid. In contrast, for the acid-oxidized CNTs, the metal particles had a broad size distribution (ca. 1.5–3.6 nm) with poor dispersion on the CNT surface (Fig. 1d and g). For the PD functionalized CNTs, PD molecules can serve as uniform nucleation centers on the CNT surface via the amino groups, which adsorb Pt and Ru precursors driven by both electrostatic interaction and coordination [27]. For the acid-oxidized CNTs, however, a large number of defects on their walls and tips make it difficult to control the size dispersion and distribution of metal particles on the CNT surface. In addition, the loading mass of Pt and PtRu NPs in the PD-CNT catalysts was determined by inductively coupled plasma-optical emission spectroscopy. The results showed that the mass content of Pt was about 18.9 wt% for the Pt/PD-CNTs, and for the PtRu/PD-CNTs, Pt and Ru were about 13.11 wt% and 5.54 wt%, respectively, both of which are closed to the designed loading amount (20 wt%).

The X-ray diffraction (XRD) patterns of PtRu/PD-CNTs and Pt/PD-CNTs are shown in Fig. 2 accompanied with PD-CNTs and Raw-CNTs as a comparison. In order to get more refined crystal structure data, scanning speed was performed at 2° per minute. Distinct diffraction peaks of the hexagonal structure of graphitic carbon in Raw-CNTs are observed in Fig. 2a (JCPDS, No. 75-1621) [31]. Compared with the characteristic diffraction peak of Raw-CNTs, the XRD pattern of the PD-CNTs shows two additional intensity peaks at $2\theta = 12.5$ and 27.6° in Fig. 2b. In the case of the Pt and PtRu NPs on PD-functionalized CNTs, the XRD peaks at *ca.* 39.9, 46.2, 67.5 and 81.5° are ascribed to (111), (200), (220) and (311) crystalline planes of the face-centered cubic (fcc) structure of Pt [32,33]. The diffraction peaks near 38° and 44° in 2θ from Ru are not observed in Fig. 2c, it is suggested that Ru enter the Pt lattice to form the PtRu alloy or Ru exists in the amorphous state [34,35]. The diffraction peaks for Pt (220) are used to estimate the Pt and PtRu NPs size with the Scherrer equation [19] because of no interference from other diffraction peaks. The average size of Pt and PtRu NPs in this system is about 2.3 and 2.0 nm respectively, which is good agreement with the values obtained by TEM analysis. The lattice parameters of Pt fcc crystal (a) were further calculated from the XRD data. The theoretical values were calculated based on Vegard's law [36], assuming $a_{Pt} = 0.3916$ nm for Pt/PD-CNTs, and $a_{PtRu} = 0.3898$ nm for PtRu/PD-CNTs. Meanwhile, the X-ray diffraction patterns of the PD, PtRu/AO-CNTs and PtRu/C are list in Supporting information Fig. S3.

3.3. FT-IR, UV–visible spectra and TGA analysis of PD-CNTs

FT-IR spectra of the (a) PD-CNTs, (b) PD and (c) PA are presented in Fig. 3. For the PD-CNTs, a broad peak at 3437 cm^{-1} is assigned to the N–H stretching vibration [37]. The two peaks at 1691 and

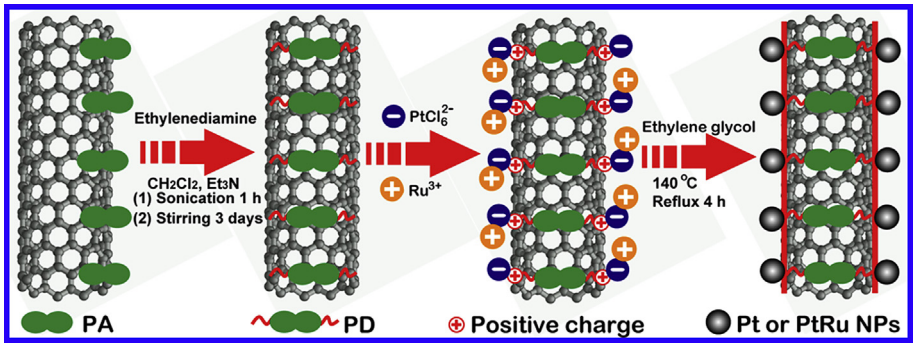

Scheme 1. Schematic diagram of the synthetic procedures of Pt and PtRu NPs on PD-functionalized CNTs.

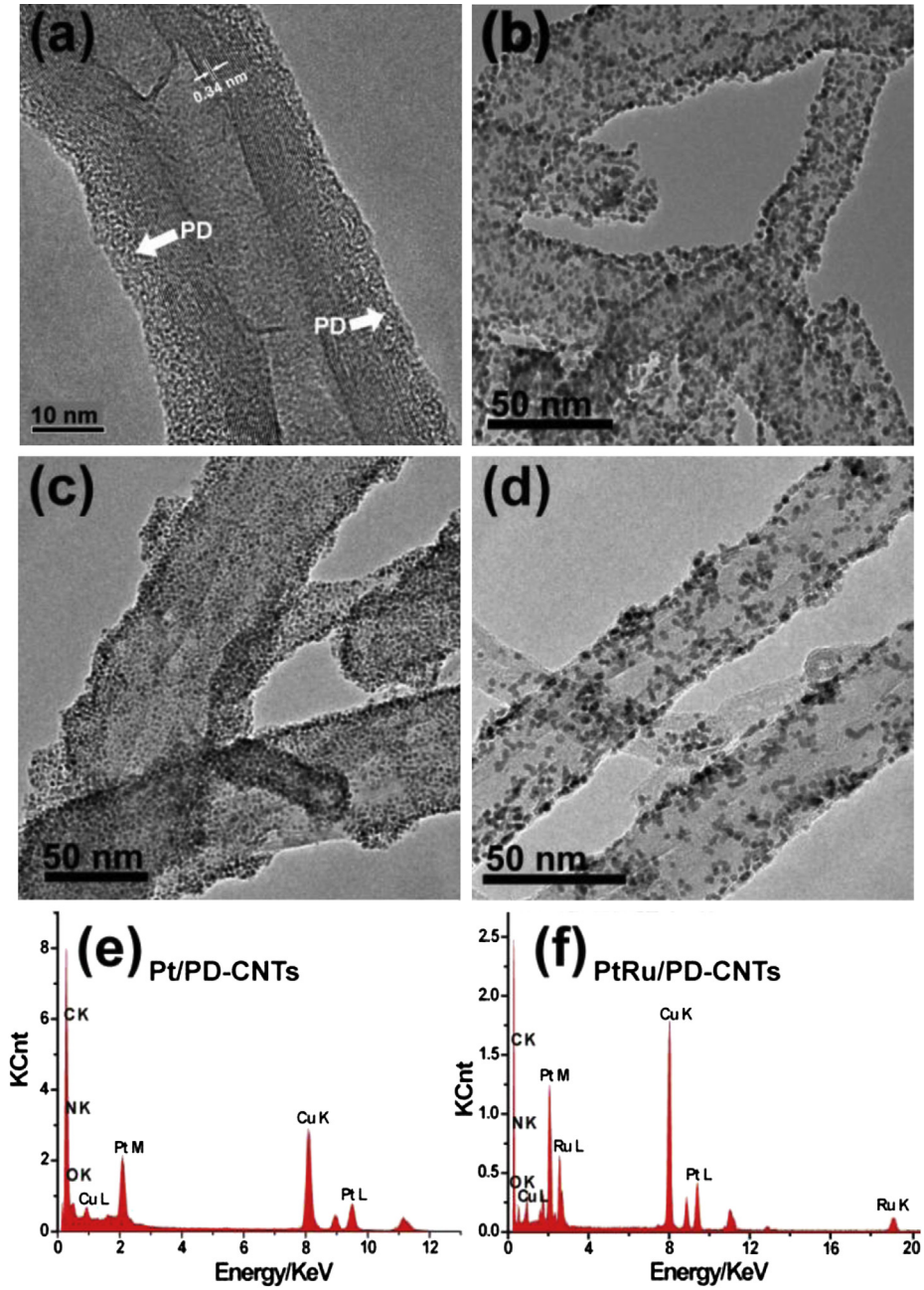

Fig. 1. (a) TEM image of PD-functionalized CNTs; (b, e) and (c, f) TEM images and EDX spectrum of Pt/PD-CNTs and PtRu/PD-CNTs respectively; (d) TEM image of PtRu/AO-CNTs.

1645 cm^{-1} due to the stretching of C=O [38], and the peak at 1589 cm^{-1} is ascribed to the C=C stretching vibration or N–H in-plane stretching in amine [21,39]. The peak at 1441 cm^{-1} is the C–H bending vibration and the peaks at 1348, 1246 and 1161 cm^{-1} can be assigned to the C–N stretching vibration and N–H bending vibration, which is a typical profile of lactam [40]. The spectrum of PD is very similar to that of the PD-CNTs, which suggest that the PD has been successfully wrapped on the surface of CNTs via π–π stacking. In addition, for the PA molecule, the peak at 1024 cm^{-1} is assigned to the C–O–C stretching vibration [8], and the very broad peak at 1774 cm^{-1} can be ascribed to the C=O stretching vibration [41]. The significant changes indicate that the PA molecule has been successfully changed into PD molecule.

A comparative study of the UV–vis spectra of PD, Raw-CNTs and PD-CNTs resolved in ethanol shows in Fig. 4. The UV–vis absorption spectrum for PD (in Fig. 4a) with the distinct bands in the ranges 416–604 nm, which is the characteristic vibronic structure associated with the π–π* transition of the PD moiety with broad maximum at 529 nm with shoulder at 494 nm [29]. The Raw-CNTs show a typical featureless spectrum in Fig. 4b. However, the absorption spectrum of PD-CNTs in Fig. 4c shows a red-shifted characteristic absorption bands between 440 and 705 nm with the main peaks at 487 and 520 nm relative to the PD moiety. The red-shift of the absorption observed for PD-CNTs is consistent with the formation of π–π stacking between the PD molecules and the six-membered rings of the sidewalls of CNTs, which is consistent with the adsorption of perylene dyes onto the sidewalls of single-walled carbon nanotubes via π–π stacking [29,30].

The weight percentage of surface-functionalized organic moieties on CNTs can be measured by TGA analysis [42,43]. For the

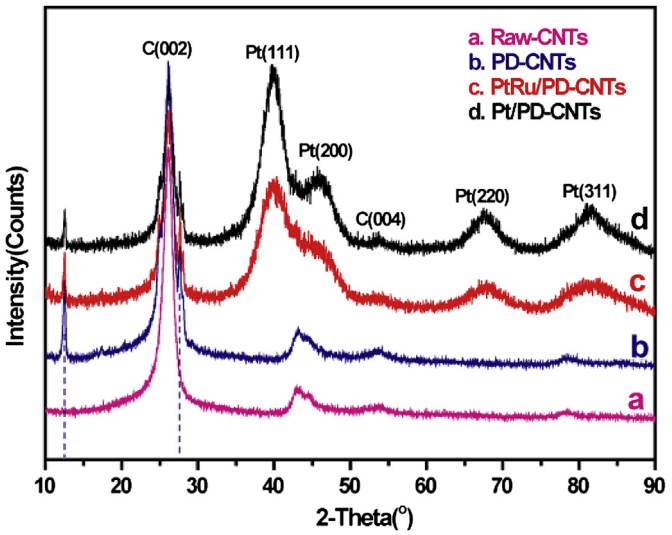

Fig. 2. X-ray diffraction patterns of (a) raw-CNT, (b) PD-CNT, (c) PtRu/PD-CNT and (d) Pt/PD-CNT composites at a scan rate of 2°/min.

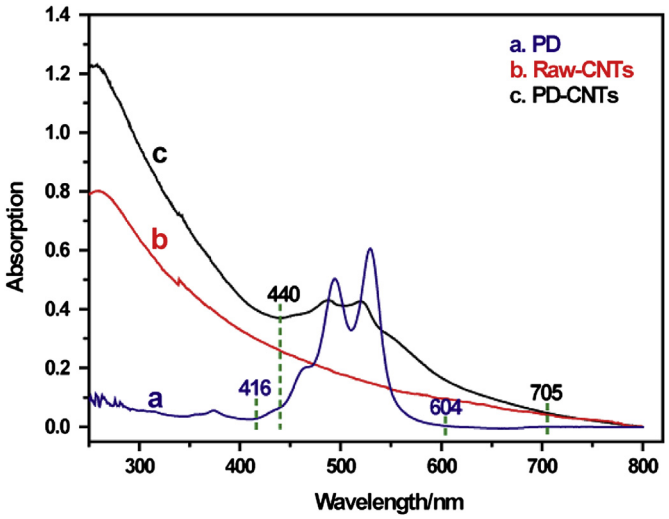

Fig. 4. UV–visible spectra of (a) PD, (b) raw-CNTs and (c) PD-CNTs.

pristine CNTs (Fig. 5a), the weight loss in the temperature range of 100–800 °C is normally attributed to amorphous carbon particles (about 5.25%) attached on CNT surfaces, while for the acid oxidation-treated CNTs (Fig. 5b), the weight loss in the same temperature range is 14.42%, which mainly attributed to –OH, –COOH and lots of amorphous carbon particles. However, for the PD molecule functionalized CNTs, the weight loss in the range of 100–800 °C should be ascribed to the pyrolysis of PD molecules besides amorphous carbon particles on the surface of CNTs (Fig. 5c). The extra weight loss of PD molecules in PD-CNT sample compared to the pristine CNTs is estimated to be ca. 4.93%.

3.4. XPS analysis of Pt and PtRu NPs on PD-CNTs

The XPS spectra of PtRu and Pt NPs on PD-CNTs and PtRu/AO-CNTs are shown in Fig. 6A. Besides the C1*s* signal at 284.8 eV, the O1*s*, Pt4*f* and Pt4*d* signals all appear in three samples. It is noteworthy that the N1*s* signal derived from PD can't be observed in the PtRu/AO-CNTs but in the PtRu/PD-CNTs and Pt/PD-CNTs. As shown in Fig. 6B, the N1*s* line was deconvoluted into four peaks at 398.7, 399.92, 400.51, and 401.83 eV. In these peaks, 399.92 and 400.51 eV are characteristic peaks for the amine-like nitrogen atoms (–NH–) [44]. The binding energy at 401.83 eV is due to the protonated ammonium ions [45,46]. The peak at 398.7 eV demonstrates the presence of Pt–N or Ru–N bonding between the N atoms of PD and the surface Pt or Ru atoms of the PtRu alloy NPs. These spectral results illustrate the bifunctional stabilizing mechanism of PD between PtRu alloy NPs and CNTs.

The Pt4*f* line of PtRu/PD-CNTs in Fig. 6C shows a doublet containing a low-energy band (Pt4$f_{7/2}$) and a high-energy band (Pt4$f_{5/2}$) at 71.65 and 74.95 eV, respectively. In order to identify different oxidation states of Pt, the spectrum was deconvoluted into two pairs of peaks at 71.57, 72.38 eV and 74.91, 76.09 eV. The more intense doublet peaks with binding energies of 71.56 eV (Pt4$f_{7/2}$) and 74.90 eV (Pt4$f_{5/2}$) are attributed to the metallic Pt, while the second deconvoluted doublets observed at higher binding energy than Pt^0 at 72.31 and 76.06 eV can be assigned to Pt^{2+} in PtO and $Pt(OH)_2$-like species [47]. Fig. 6D shows the Ru3*p* region of the PtRu/PD-CNT catalyst. Due to the Ru3*d* peaks overlap with the C1*s*

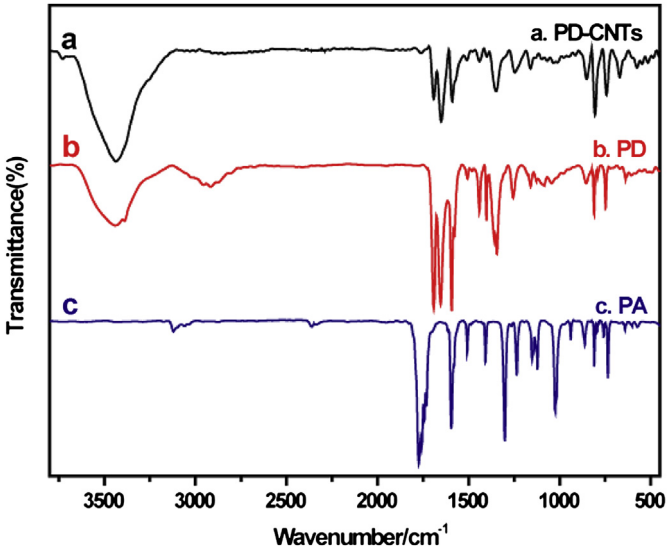

Fig. 3. FT-IR spectra of (a) PD-CNTs, (b) PD and (c) PA.

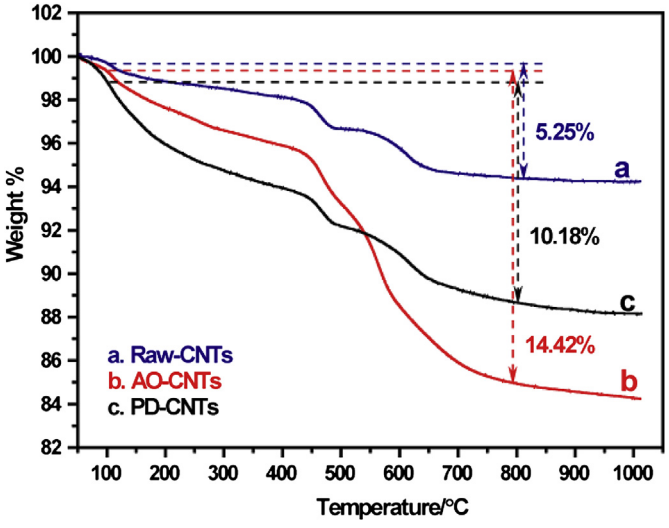

Fig. 5. TGA weight loss curves of (a) raw-CNTs, (b) AO-CNTs and (c) PD-CNTs.

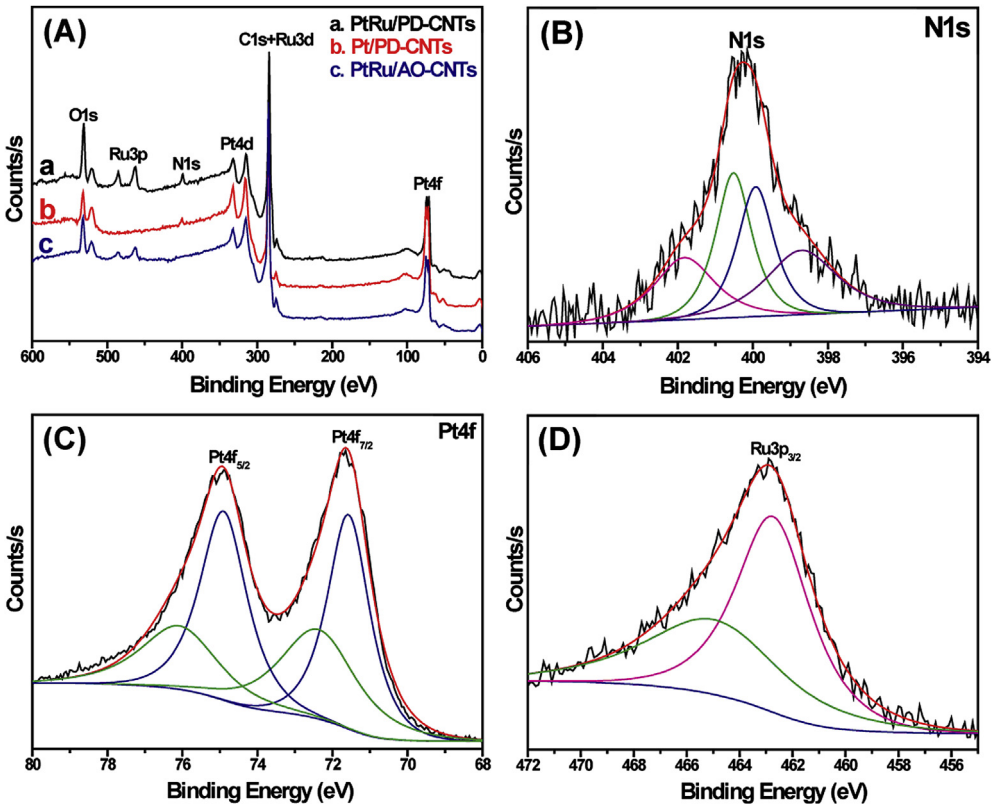

Fig. 6. XPS spectrum of PtRu/PD-CNTs and PtRu/AO-CNTs (A), XPS spectrum of N1*s* (B), Pt4*f* (C) and Ru3$p_{3/2}$ (D) of PtRu/PD-CNTs.

peak, the Ru3*p* spectrum is chosen for the analysis of the Ru oxidation state. The Ru3$p_{3/2}$ signal could be deconvoluted into two distinguishable peaks of different intensities located at 462.74 and 464.98 eV, which corresponded well with metallic Ru and RuO_2 species, respectively [48,49]. Pt and Ru peak positions observed for PtRu/AO-CNTs (see Supporting information Fig. S4) were similar to the PtRu/PD-CNTs, and to those reported in the literature for PtRu on CNTs [50,51].

3.5. The electrochemical surface area of the catalysts

CO stripping voltammetry is measured to characterize the electrochemical active surface (EAS) areas of Pt and PtRu NPs on PD-functionalized CNTs in Fig. 7. Compared to CV measurement, CO stripping is more feasible to determine the EAS areas of Pt and PtRu NPs with low loading quantity, considering the weak electrical signals from the desorption of hydrogen atoms bonded on Pt surfaces and the uncertainty introduced by the background current subtraction [52]. It is well known that the CO molecules adsorb on Pt surface in a linear one-to-one bonding form. For simplicity, it is assumed that the same behavior happened on surface of PtRu catalysts [53]. In CO stripping, CO initially adsorbed on Pt and PtRu NPs will be oxidized to CO_2 in the subsequent scans. The EAS areas of Pt and PtRu NPs were calculated based on the CO stripping voltammetry, assuming that the oxidation of a CO monolayer adsorbed on 1 cm^2 of Pt or PtRu requires 0.42 mC [52]. Consequently, the EAS areas of PtRu/PD-CNT and Pt/PD-CNT catalysts are calculated for 156.2 $m^2\ g^{-1}$ and 67.2 $m^2\ g^{-1}$ respectively. For easy to compare, the CO stripping voltammetry of the as-prepared PtRu NPs on acid-oxidized CNTs and carbon black were also investigated as shown in Supporting information Fig. S5.

3.6. Evaluation of methanol electro-oxidation

The catalytic activity of the prepared Pt and PtRu NPs on PD-CNTs toward methanol oxidation was evaluated in an electrochemical measurement system using that of PtRu NPs on AO-CNTs and carbon black as comparison. The methanol oxidation activity is reflected by the magnitude of the anodic peak current in the forward scan, while the peak in the reverse scan is originated from the reactivation of Pt associated with the removal of the residual carbon species [54]. Fig. 8A shows CVs of methanol oxidation in 0.5 M H_2SO_4 containing 1.0 M methanol. It can be seen that the methanol oxidation on PtRu/

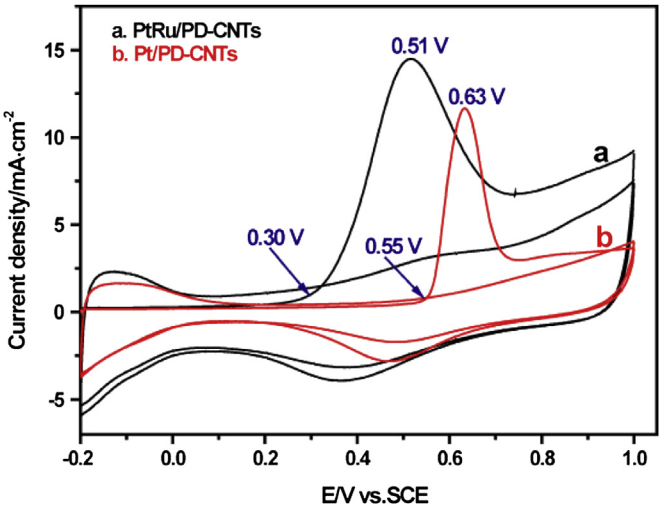

Fig. 7. CO stripping voltammograms of (a) PtRu/PD-CNT and (b) Pt/PD-CNT catalysts in 0.5 M H_2SO_4 at room temperature and 50 mV s^{-1} scan rate.

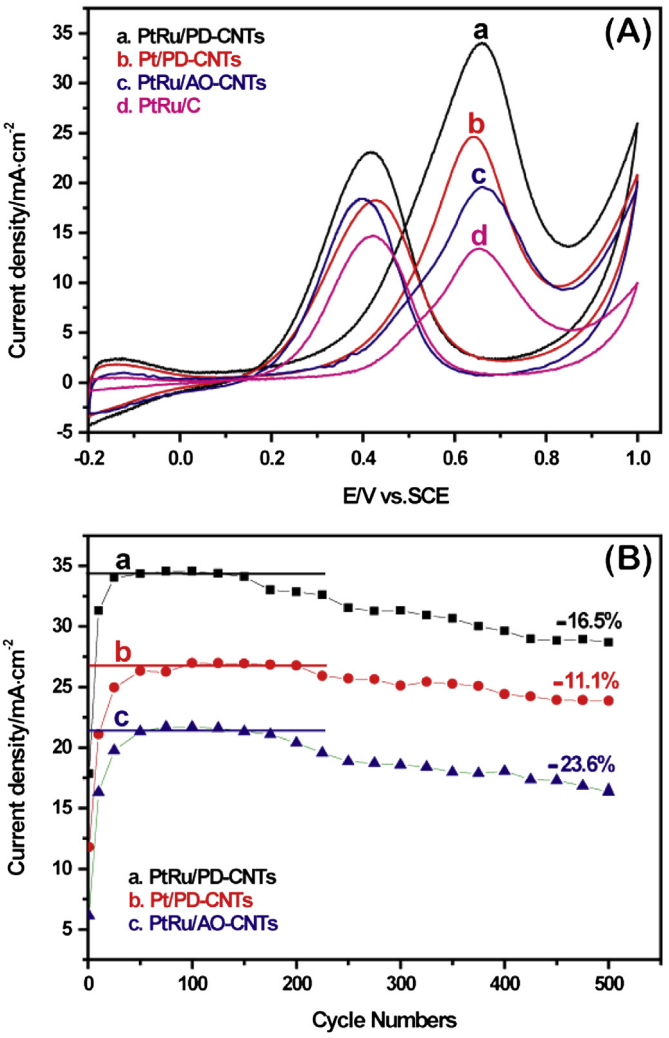

Fig. 8. (A) Cyclic voltammograms of (a) PtRu/PD-CNT, (b) Pt/PD-CNT, (c)PtRu/AO-CNT and (d) PtRu/C catalysts in nitrogen-saturated 0.5 M H_2SO_4 + 1.0 M CH_3OH at a scan rate of 50 mV s^{-1}. (B) Long-term cycle stabilities of (a) PtRu/PD-CNT, Pt/PD-CNT and PtRu/AO-CNT catalysts in 0.5 M H_2SO_4 + 1.0 M CH_3OH aqueous solution.

PD-CNTs started at about 0.25 V, which is significantly lower than the onset voltage for Pt/PD-CNTs (0.30 V), PtRu/AO-CNTs (0.33 V) and PtRu/C (0.37 V). Moreover, in the forward potential scan, the peak current density on PtRu/PD-CNT catalyst is 34.06 mA cm^{-2}, ~1.38-fold higher than that on Pt/PD-CNTs (24.64 mA cm^{-2}), ~1.74-fold higher than that on PtRu/AO-CNTs (19.60 mA cm^{-2}) and ~2.54-fold higher than that on PtRu/C (13.41 mA cm^{-2}). This result implies PtRu/PD-CNT and Pt/PD-CNT catalysts possess better catalytic activity than PtRu/AO-CNTs and PtRu/C in the oxidation of methanol. As mentioned above, the anodic peak in the backward scan indicates the removal of CO-like carbonaceous species, which are not completely oxidized and accumulated on the catalyst surface during the forward scan [55]. So the ratio of I_f/I_b can be used as an indicator of the CO-tolerance. That is, a higher I_f/I_b value means more completely oxidation of methanol to the final product (CO_2) during the forward anodic scan. As calculated from Fig. 8A, the PtRu and Pt NPs on PD-CNT catalysts have a much higher I_f/I_b value (1.52 and 1.35 respectively) than the PtRu/AO-CNT (1.06) and PtRu/C (0.91) catalysts, confirming that methanol molecules can be far more effectively oxidized to CO_2 on PtRu/PD-CNT and Pt/PD-CNT catalysts.

As the durability of the electrocatalysts at the anodic has been recognized as one of the most important issues for fuel cells, we also evaluate the durability of the PtRu and Pt NPs on PD-CNT and PtRu/AO-CNT catalysts through repeated CV cycles performed from −0.2–1.0 V in N_2-saturated 0.5 M H_2SO_4 consisting of 1.0 M methanol. Fig. 8B exhibits the change of peak current density of the forward scan for methanol electro-oxidation with cycle numbers. For Pt and PtRu electrocatalysts on CNTs, the forward peak current density increases initially. In the case of PtRu/PD-CNTs and PtRu/AO-CNTs, the peak current density remains almost constants from the 50th cycle to the 150th cycle after the initial increase. Using the maximum balance of current density as the reference, the reduction of the anodic peak current density at the 500th cycle for the methanol electro-oxidation on PtRu/PD-CNTs is about 16.5%, which is lower than that on PtRu/AO-CNTs (ca. 23.6%). However, for the Pt/PD-CNT catalyst, the reduction of peak current density is about 11.1%, which is apparently higher than that PtRu NPs on PD-CNTs and AO-CNTs. The high anodic peak current density and much slower degradation for methanol electro-oxidation on PtRu/PD-CNTs and Pt/PD-CNTs as compared with that on PtRu/AO-CNTs demonstrate that PD molecules on CNTs can efficiently disperse the metal NPs and reduce the particles size of metal NPs, meanwhile, PD molecules as interlinkers between metal NPs and CNTs is stronger than AO-CNTs. This strong interaction can effectively inhibit the aggregation of the metal NPs on CNTs. Compared with Pt/PD-CNT catalyst, greater proportion of reduction happened on the PtRu/PD-CNT catalyst can be deduced from dissolution of ruthenium during the oxidation of methanol [56]. The above results demonstrated that the PD molecules functionalized noncovalently CNT system is very promising potential catalyst supports for fuel cells with highly efficiency.

4. Conclusions

In summary, a new method to synthesize metal NPs/CNT catalysts using PD as a bridge between metal NPs and CNTs has been successfully developed. PD molecules with π-conjugated structure stacking on the CNTs can serve as active sites to anchor metal particles so that a desired distribution of Pt and PtRu NPs with uniform particle size was realized via electrostatic self-assembly. Cyclic voltammetry and endurance tests show that the as-prepared Pt and PtRu/PD-CNT hybrid catalysts possess both high electrocatalytic activity and excellent stability toward methanol electro-oxidation. The PD-CNT composites are proposed to be very promising potential catalyst supports for fuel cells with highly efficiency.

Acknowledgments

This work is supported by the National Natural Science Foundation of China (No. 21121063, 21273006, 91027018) and National Basic Research Program (No. 2012CB932900, 2011CB933700).

Appendix A. Supplementary material

Supplementary material related to this article can be found at http://dx.doi.org/10.1016/j.jpowsour.2013.04.084.

References

[1] S.M. Alia, K. Duong, T. Liu, K. Jensen, Y. Yan, ChemSusChem 5 (2012) 1619–1624.
[2] C. Alegre, L. Calvillo, R. Moliner, J.A. González-Expósito, O. Guillén-Villafuerte, M.V.M. Huerta, E. Pastor, M.J. Lázaro, J. Power Sources 196 (2011) 4226–4235.
[3] H. Yang, J. Zhang, K. Sun, S. Zou, J. Fang, Angew. Chem. Int. Ed. 49 (2010) 6848–6851.
[4] A.J. Martín, A.M. Chaparro, L. Daza, J. Power Sources 196 (2011) 4187–4192.
[5] H. Wu, H. Li, Y. Zhai, X. Xu, Y. Jin, Adv. Mater. 24 (2012) 1594–1597.
[6] Y. Huang, J. Cai, S. Zheng, Y. Guo, J. Power Sources 210 (2012) 81–85.
[7] M.J. Lázaro, V. Celorrio, L. Calvillo, E. Pastor, R. Moliner, J. Power Sources 196 (2011) 4236–4241.

[8] Y. Zhao, X. Yang, L. Zhan, S. Ou, J. Tian, J. Mater. Chem. 21 (2011) 4257–4263.
[9] J.E. Weaver, M.R. Dasari, A. Datar, S. Talapatra, P. Kohli, ACS Nano 4 (2010) 6883–6893.
[10] R. Bhowmick, S. Rajasekaran, D. Friebel, C. Beasley, L. Jiao, H. Ogasawara, H. Dai, B. Clemens, A. Nilsson, J. Am. Chem. Soc. 133 (2011) 5580–5586.
[11] L. De Luca, A. Donato, S. Santangelo, G. Faggio, G. Messina, N. Donato, G. Neri, Int. J. Hydrogen Energy 37 (2012) 1842–1851.
[12] S. Wang, D. Yu, L. Dai, J. Am. Chem. Soc. 133 (2011) 5182–5185.
[13] Z. Liu, B. Han, Adv. Mater. 21 (2009) 825–829.
[14] Z.D. Wei, C. Yan, Y. Tan, L. Li, C.X. Sun, Z.G. Shao, P.K. Shen, H.W. Dong, J. Phys. Chem. C 112 (2008) 2671–2677.
[15] C. Bosch-Navarro, E. Coronado, C. Martí-Gastaldo, B. Rodríguez-González, L.M. Liz-Marzán, Adv. Funct. Mater. 22 (2012) 979–988.
[16] C. Aprile, R. Martiín, M. Alvaro, H. Garcia, J.C. Scaiano, Chem. Mater. 21 (2009) 884–890.
[17] M.K. Bayazit, L.S. Clarke, K.S. Coleman, N. Clarke, J. Am. Chem. Soc. 132 (2010) 15814–15819.
[18] T. Fujigaya, S. Haraguchi, T. Fukumaru, N. Nakashima, Adv. Mater. 20 (2008) 2151–2155.
[19] Y. Zhao, X. Yang, J. Tian, F. Wang, L. Zhan, J. Power Sources 195 (2010) 4634–4640.
[20] X. Li, Y. Liu, L. Fu, L. Cao, D. Wei, Y. Wang, Adv. Funct. Mater. 16 (2006) 2431–2437.
[21] B. Wu, D. Hu, Y. Kuang, Y. Yu, X. Zhang, J. Chen, Chem. Commun. 47 (2011) 5253–5255.
[22] D. Hulicova-Jurcakova, M. Seredych, G.Q. Lu, T.J. Bandosz, Adv. Funct. Mater. 19 (2009) 438–447.
[23] J. Liang, Y. Zheng, J. Chen, J. Liu, D. Hulicova-Jurcakova, M. Jaroniec, S.Z. Qiao, Angew. Chem. Int. Ed. 51 (2012) 3892–3896.
[24] Z. Tian, C.K. Poh, Z. Wang, S.H. Lim, Z. Liu, J. Lin, Chem. Mater. 22 (2010) 832–839.
[25] Y. Tang, B.L. Allen, D.R. Kauffman, A. Star, J. Am. Chem. Soc. 131 (2009) 13200–13201.
[26] W. Xiong, F. Du, Y. Liu, A. Perez, M. Supp, T.S. Ramakrishnan, L. Dai, L. Jiang, J. Am. Chem. Soc. 132 (2010) 15839–15841.
[27] B. Wu, D. Hu, Y. Kuang, B. Liu, X. Zhang, J. Chen, Angew. Chem. Int. Ed. 48 (2009) 4751–4754.
[28] F. Li, H. Yang, C. Shan, Q. Zhang, D. Han, A. Ivaska, L. Niu, J. Mater. Chem. 19 (2009) 4022–4025.
[29] W. Feng, A. Fujii, M. Ozaki, K. Yoshino, Carbon 43 (2005) 2501–2507.
[30] C. Ehli, C. Oelsner, D.M. Guldi, A. Mateo-Alonso, M. Prato, C. Schmidt, C. Backes, F. Hauke, A. Hirsch, Nat. Chem. 1 (2009) 243–249.
[31] D. Sebastián, A.G. Ruíz, I. Suelves, R. Moliner, M.J. Lázaro, V. Baglio, A. Stassi, A.S. Aricò, Appl. Catal. B: Environ. 115–116 (2012) 269–275.
[32] Z.-H. Lin, Z.-Y. Shih, H.-Y. Tsai, H.-T. Chang, Green Chem. 13 (2011) 1029–1035.
[33] J. Wu, J. Zhang, Z. Peng, S. Yang, F.T. Wagner, H. Yang, J. Am. Chem. Soc. 132 (2010) 4984–4985.
[34] J.T. Moore, J.D. Corn, D. Chu, R. Jiang, D.L. Boxall, E.A. Kenik, C.M. Lukehart, Chem. Mater. 15 (2003) 3320–3325.
[35] Z. Cui, C. Liu, J. Liao, W. Xing, Electrochim. Acta 53 (2008) 7807–7811.
[36] X. Yang, J. Zheng, M. Zhen, X. Meng, F. Jiang, T. Wang, C. Shu, L. Jiang, C. Wang, Appl. Catal. B Environ. 121–122 (2012) 57–64.
[37] Y. Jalit, M.C. Rodríguez, M.D. Rubianes, S. Bollo, G.A. Rivas, Electroanalysis 20 (2008) 1623–1631.
[38] H.J. Salavagione, J. Arias, P. Garcés, E. Morallón, C. Barbero, J.L. Vázquez, J. Electroanal. Chem. 565 (2004) 375–383.
[39] L. Lai, L. Chen, D. Zhan, L. Sun, J. Liu, S.H. Lim, C.K. Poh, Z. Shen, J. Lin, Carbon 49 (2011) 3250–3257.
[40] Y. Zhao, X. Yang, J. Tian, Electrochim. Acta 54 (2009) 7114–7120.
[41] J.-H. Lee, S.-M. Yoon, K.K. Kim, I.-S. Cha, Y.J. Park, J.-Y. Choi, Y.H. Lee, U. Paik, J. Phys. Chem. C 112 (2008) 15267–15273.
[42] Y.L. Hsin, K.C. Hwang, C.-T. Yeh, J. Am. Chem. Soc. 129 (2007) 9999–10010.
[43] I. Kalinina, K. Worsley, C. Lugo, S. Mandal, E. Bekyarova, R.C. Haddon, Chem. Mater. 23 (2011) 1246–1253.
[44] D. He, C. Zeng, C. Xu, N. Cheng, H. Li, S. Mu, M. Pan, Langmuir 27 (2011) 5582–5588.
[45] W.-F. Chen, J.-S. Wu, P.-L. Kuo, Chem. Mater. 20 (2008) 5756–5767.
[46] P. Zhang, J. Li, D. Liu, Y. Qin, Z.-X. Guo, D. Zhu, Langmuir 20 (2004) 1466–1472.
[47] R. Chetty, S. Kundu, W. Xia, M. Bron, W. Schuhmann, V. Chirila, W. Brandl, T. Reinecke, M. Muhler, Electrochim. Acta 54 (2009) 4208–4215.
[48] Y. Liang, J. Li, Q.-C. Xu, R.-Z. Hu, J.-D. Lin, D.-W. Liao, J. Alloys Compd. 465 (2008) 296–304.
[49] F. Şen, G. Gökğaç, Energy Fuels 22 (2008) 1858–1864.
[50] Z. Sun, X. Wang, Z. Liu, H. Zhang, P. Yu, L. Mao, Langmuir 26 (2010) 12383–12389.
[51] N.-Y. Hsu, C.-C. Chien, K.-T. Jeng, Appl. Catal. B Environ. 84 (2008) 196–203.
[52] Z. Guo, Y. Chen, L. Li, X. Wang, G.L. Haller, Y. Yang, J. Catal. 276 (2010) 314–326.
[53] L. Ren, Y. Xing, Electrochim. Acta 53 (2008) 5563–5568.
[54] F. Su, Z. Tian, C.K. Poh, Z. Wang, S.H. Lim, Z. Liu, J. Lin, Chem. Mater. 22 (2009) 832–839.
[55] L. Kuai, S. Wang, B. Geng, Chem. Commun. 47 (2011) 6093–6095.
[56] D.-J. Guo, J.-M. You, J. Power Sources 198 (2012) 127–131.